Lawrence Berkeley National Laboratory

Title
Anion Exchange Ionomers: Impact of Chemistry on Thin-Film Properties

Authors
Luo, Xiaoyan
Kushner, Douglas I
Li, Jonathan
et al.

Anion Exchange Ionomers: Impact of Chemistry on Thin-Film Properties

Xiaoyan Luo, Douglas I. Kushner, Jonathan Li, Eun Joo Park, Yu Seung Kim, Ahmet Kusoglu*

Dr. X. Luo, Dr. D. I. Kushner, J. Li, and Dr. A. Kusoglu
Energy Technologies Area, Lawrence Berkeley National Laboratory, 1 Cyclotron Road, Berkeley CA 94720, USA
* Email: AKusoglu@lbl.gov

J. Li
Department of Materials Science & Engineering, University of Michigan, 2300 Hayward Road, Ann Arbor, MI 48109, USA

Dr. E. J. Park and Dr. Y. S. Kim
MPA-11: Materials Synthesis and Integrated Devices, Los Alamos National Laboratory, Los Alamos NM 87545, USA

Abstract: Ionomer thin-films (i.e., 20-100 nm) on supports serve as model systems to understand ionomer-catalyst interfacial behavior as well as the confinement-driven deviation in properties from bulk membranes. While ionomer thin-films have been examined for proton-exchange ionomers (PEIs), the thin-film properties of anion exchange ionomers (AEIs) remain largely unexplored. More importantly, delineating the convoluted impact of chemistry and confinement on thin-film morphology and hydration is of interest to advancing the field on functional ionic interfaces. In this work, we systematically study these aspects by using AEIs of different backbones (perfluorinated, aliphatic, and aromatic) and side chains (various lengths, and single vs. dual functional groups). Quartz-crystal microbalance and spectroscopic ellipsometry are used to analyze density and coupled with calculated free volume fraction of thin-films to provide insights on their gas transport properties. AEI side-chain's chemical character plays a key role on how confinement modulates the hydration (in thin-film vs. bulk). Our results elucidate the effects of backbone, side-chain chemistry vs. anion/cation type in the confinement-driven changes in thin-film morphology and swelling. This study also provides new insights for tuning AEI transport functionalities at interfaces via chemistry, which could benefit design and development of electrode-ionomers for alkaline membrane-based energy systems.

1. Introduction

Anion-exchange membrane fuel cells (AEMFC) and water electrolyzers (AEMWE) are emerging hydrogen production and utilization technologies as they can utilize non-noble metal catalysts, cheaper ionomers and afford greater fuel flexibility to drive down the system cost, providing advantages over conventional proton-exchange membrane-based fuel cells (PEMFCs) and electrolyzers (PEMWE).[1] However, a majority of AEMFC and AEMWE reported in the literature was unable to achieve high current density until very recently due to lack of understanding of ionomer-catalyst interface.[2] [3]Similar to the PEM based devices, electrodes in the AEM-based devices utilize thin ionomer films in their catalyst layer, which not only transport the hydroxide ions and gaseous hydrogen and oxygen but also accommodate the significant amount of water in the catalyst layers (CLs).[1-2] Thus, ionomers on the anode and cathode require proper handling of water to produce high current density. For example, an asymmetric cell with different ionomers on two electrodes demonstrated the viability of high-performance and durable AEMFCs under low RH and high current generating conditions.[4] Moreover, water sorption and swelling of the thin anion-exchange ionomer (AEI) layer are coupled to its catalyst binding ability, which is critical to the stable operation of the AEM-based devices.[5]

In the past decade, the fields of AEM-based devices have witnessed a strong interest in related research activities. Much attention has been centered on the development of new quaternized polymer chemistries with high anion conductivity [6] and good chemical stability under high pH,[2b, 7] and electro-oxidative conditions. [8] A silver-catalyzed AEMFC using a quaternized poly(arylpiperidinium) (PAP) showed high peak power density of 0.92 W cm^{-2}.[9] Radiation-grafted poly(ethylene-*co*-tetrafluoroethylene)-(ETFE)-based AEIs possess hydroxide conductivity of 200 mS cm^{-1} and the AEMFC using the AEM achieved 2 W cm^{-2} peak power density at 80 °C.[10] Aryl ether-free polyaromatic AEIs exhibited promising performance, *ca.*1.5 W cm^{-2} power density.[11] Recently, highly quaternized polystyrene AEIs showed excellent water electrolyzer performance (current density of 5 A cm^{-2} at 1.8 V), approaching the state-of-the-art PEM electrolyzer.[5, 12] Besides the hydrocarbon AEIs,

perfluorinated AEIs were developed to potentially harness excellent chemical stability and high conductivity of perfluorinated chemistry and showed comparable fuel cell performance.[13] To date, significant progress to improve the hydroxide conductivity of quaternized polymers has been made. Increasing hydroxide conductivity is critical to reducing cell ohmic resistance; however, the impact of the chemistry of AEI on thin-film (i.e., 20-100 nm) properties such as morphology, hydration, and transport is unclear. There is a strong need for research to study AEI thin-film systematically for further performance and durability improvement of the AEM-based devices.

A growing number of recent studies on PEM thin-films have outlined the dramatic changes occurring in ionomer structure when it is confined to nanometer thicknesses on supporting substrates accompanied with reductions in water uptake, swelling, oxygen transport, and proton conductivity.[14] In most of these studies, perfluorosulfonic acid (PFSA) ionomer thin-film on a homogeneous substrate were served as model systems for catalyst ionomers and enabled the utilization of various characterization techniques, such as ellipsometry, grazing-incidence X-ray scattering (GISAXS), and neutron reflectivity.[14a] Findings from these studies confirmed the confinement-driven changes in PFSA ionomers and elucidated the origins of transport resistances observed in the cathode catalyst layers of PEMFC. While the characterization of PEM thin-films has been proven to be critical for understanding the origins of transport limitations in catalyst layers and mitigating the resulting performance losses in PEM-systems, such efforts are yet to be undertaken for AEMs. Thin-films also serve as an analog for understanding the interfacial phenomena occurring in bulk membranes.[15] For example, the presence of an interfacial skin layer hypothesized at the polymer-air interface of bulk PFSA membranes was suggested to be the bottleneck of water permeation through the membrane and could be understood by studying these ionomers in thin-film form.[16] However, only a few papers studied AEMs in thin-film form[17] with earlier efforts focusing on former commercially available AEMs such as Tokuyama® A201 (no longer available). Compared to Nafion thin-films, Tokuyama thin-films showed lower water sorption, and its solvation occurred at higher relative humidity.[17b] Quaternized comb-shaped poly(p-phenylene oxide)

(QA-PPO) thin-films exhibit a confinement effect accompanied by a different water sorption mechanism compared to their bulk membrane counterparts.[17a] Nevertheless, nascent characterization of AEIs confined to nanometer-thick films limits the current state of understanding. In particular, moving from PEMFC to AEMFC systems not only alters the pH environment and electrochemistry but also limits the library of ionomer chemistries available to understand differing structure-property-function relationships.

Thus, fundamental questions remain as to how backbone and side-chain chemistry (i.e., aliphatic vs. aromatic, fluorinated vs. hydrocarbon, and short vs. long side-chain) of an ionomer governs their properties, especially in the thin-film motif. Among the features of particular interest in these energy applications that involve water management are hydrated morphology, swelling, and water uptake.

To this end, the objective of this work is to investigate properties of AEI thin-films of various chemistries (Figure 1, Fumion is omitted due to lack of public disclosure) and establish correlations between their properties. We provide critical AEI design parameters where possible.

2. Results

2.1 Morphology

Figure 2 shows the nano-morphology scattering patterns of the thin-films under ambient humidity (35% RH) and near vapor-saturated conditions (95% RH) with GISAXS. The only samples that show detectable phase-separation were two perfluorinated polymers (PF-AEM and PFSA), while the hydrocarbon-based thin-film samples were amorphous regardless of film thickness (Figure S2). It is important to note that no strong preferential nano-domain orientation is observed in PF-AEM, even though it has slightly larger domain spacing in the plane of the thin-film (5.6-5.9 nm) than that for PFSA thin film (domain spacing ~ 4-5 nm). Likely, these features could also be affected by substrate type (i.e., metallic vs dielectric); however, it is unclear how the presence of the quaternary ammonium will affect

interactions with metallic substrates as has been shown with sulfonated polymers on metallic substrates.[18]

Phase separation of polymers is driven by the enthalpy of mixing between incompatible components of the polymer (e.g., a hydrophilic side chain bound to a hydrophobic backbone in PFSAs).[19] Electrostatic interactions between charged regions were proposed to favor agglomeration, forming phase-separated ionic clusters.[20] Thus, the extent of ionic cluster formation and degree of phase-separation is controlled by (i) the strength of the electrostatic interactions between the ion pairs, (ii) stiffness of the host matrix,[20] and (iii) side chain mobility. The strength of the electrostatic interactions among AEI is more or less similar as all ammonium functional groups are alkyl ammonium except PAP-BP-60. Typically, chain stiffness governs mechanical and thermal properties while also affecting the ability of a polymer to phase separate as the backbone becomes less able to contort in orientations that would permit side-chain aggregation, allowing thermal properties to act as a proxy for the ability to aggregate. Host polymers of perfluorinated and polystyrene, which are aliphatic, have significantly lower T_α, ~ 100 °C (i.e., the "glass" transition temperature at which polymer enters into a rubbery state with increased segmental mobility .) than the rest of other host polymers, such as poly(p-phenylene oxide) based ionomers (QA-PPO and Fumion), which are aromatic, with T_α ~200 °C. Therefore, Nafion, PF-AEM, and polystyrene-based ionomers are expected to have a stronger tendency to phase-separate at the nanoscale. However, polystyrene-based ionomers show a much weaker phase-separation owing to their stiffer side-chain structure than perfluorinated ionomers. Thus, collectively, lower T_α of host polymer along with the higher side-chain mobility in PF-AEM and Nafion could explain why these two perfluorinated ionomers show nano-phase separation regardless of the type of ions.

2.2 Swelling Behavior

Hydration of thin-films is summarized in Figure 3 in terms of thickness swelling with relative humidity (RH). All AEI films tested in this work show higher swelling than the Nafion film, which acts as the baseline ionomer due to the prevalence of published analysis and results. It was known that IEC

strongly affects ionomer swelling for PFSA in both bulk and thin-film forms.[14a, 15a] If one assumes that

IEC is the primary parameter governing the swelling, then a correlation between maximum swelling and

IEC is expected. However, as shown in Figure S3, thickness swelling as a function of IEC does not

show a strong correlation, motivating the need for exploring factors beyond IEC that control the

ionomer swelling, such as structure, counter-ion, and chemistry within the AEM class of polymers. For

example, extracted swelling data from a series of QA-PPO ionomer thin films[17a] show that C16D40

exhibits similar swelling to Nafion while having 1.6× the IEC; this is likely due to the crystallization of

the alkyl side chains creating a high swelling counterforce.

To examine the different aspects that govern swelling, solubility parameters, δ, of ionomers using the

group contribution method were calculated. Historically, using group contribution methods allows for

estimation of various polymer properties (e.g., adhesive energy, critical temperature, critical volume,

solubility) with good accuracy and applicability, although the caveat that the solubility parameters for

charged ionomer systems remain largely unexplored.[21] Solubility parameters is determined from the

following expression based on the group contribution method:[22]

$$\delta = (\frac{\Delta E_V}{V})^{1/2} \tag{1}$$

where ΔE_V is vaporization energy and V is the total molar volume of the polymer repeat unit,

determined from the groups contributing to the solubility parameter using Fedors' cohesion

parameter.[22]

The solubility parameters, δ are plotted in Figure S 3 (see SI for details).[22] Nafion possesses the lowest

δ, while PSS has the highest solubility parameter of 28.7 MPa$^{1/2}$ – a value that agrees well with previous

reports.[23] When swelling is plotted against δ as shown in Figure 4a, the degree of swelling shows an

increase trend as δ approaches ~~that of water (δ= 48~~ 30 MPa$^{1/2}$ (see Figure S 3 for additional

correlations). It is interesting to note that the correlation between swelling vs. IEC is relatively poor

(Figure S 3). In other words, the swelling of the thin-film is affected not only IEC but also the chemical

structure of ionomer. For example, PSS, with the closest δ (30 MPa$^{1/2}$) to water (48 MPa$^{1/2}$), attains the

largest swelling, compared to all samples. For the QA-PPO films, increasing alkyl side-chain length from 0 to 16 carbons results in reduced δ accompanied by a reduction in swelling. Scattering in the correlations in the swelling vs. solubility parameter suggests that free volume contributes an additional role in swelling.

Compared to QS, N2-25 possesses one additional quaternary ammonium on its side-chain and higher δ, which leads to higher swelling and water content, as shown in Figure 4b. This is similar to the PFSA-based thin-films in acid-form,[24] when another acid group is added to the side-chain in a perfluorosulfonic imide acid ionomer,[25] it shows higher water uptake than its PFSA analogue with single acid end group. Despite a lack of significant morphological changes with hydration, swelling of the ionomers with flexible polymer backbones (N2-25, and PSS) increases substantially at high RH, owing to their ability to accommodate more water molecules.

2.3 Ionomer Density and Free Volume

The free volume of the polymers is an important parameter for gas and water diffusion functionality (as in electrode films), but it is relatively difficult to directly measure in thin-films.[26] Polymer density is known to be inversely proportional to its free volume[27] and thus used as a proxy. In this study, QCM and ellipsometry were coupled to derive the dry density (ρ_p) of AEI thin-films on substrate. Figure 5 shows ρ_p values calculated from the slope of a plot of thickness swelling vs. water mass uptake of the thin-films (details can be found in SI). PFSA film in the dry state has a density (ρ_p) of 1.9 g cm^{-3}, which is consistent with previous reports for this class of polymer.[14a, 16, 28] To complement the measured data, we also used the group contribution method to estimate polymer density. The molar mass and volume values of each contributed group were taken from ref. [29]

$$\rho = \frac{molar\ mass\ (g\ mol^{-1})}{molar\ volume\ (L\ mol^{-1})} \qquad (2)$$

(See SI for an analysis of the calculated density values in comparison to apparent density estimated from QCM and ellipsometry, Figure S5). Looking further into Figure 5, ρ_p of QA-PPO decreases with increasing the length of the side-chain. QS and N-25 show lower ρ_p than QA-PPO, which indicates that AEIs with polystyrene (PS) backbone could have a larger free volume.

To further study this prediction, we determine the free volume fraction (FVF) of ionomer film using:

$$FVF = \frac{V - 1.3 \times V_{vdW}}{V} \tag{3}$$

where V is the total volume and V_{vdW} is the van der Waals volume of polymers estimated by the Bondi group contribution method[29-30], respectively.

A plot of FVF vs. ionomer density shows an inverse relationship (Figure 5), as expected and in agreement with the literature.[27] In addition, the FVF calculations validate our prediction that polymers with a polystyrene backbone like QS and N2-25 have a larger free volume over the aromatic backbone polymers tested. These measurements provide compelling evidence for the role of chemistry in tuning ionomer film's free volume, which could be an useful factor for designing anion-exchange materials for electrodes with optimized mass transport properties.

2.4 Confinement Effect on Hydration

The role of nano-confinement on controlling hydration behavior of proton-exchange thin-films is significant.[15] Generally, strong confinement was observed in PFSA thin-films cast on supporting substrates, meaning thin-films show a lower water content than their free-standing bulk membrane counterpart ($\lambda_{bulk} > \lambda_{film}$). Figure 6 shows comparisons of RH-dependent water content in thin-films to their bulk membrane analogs. Figure 7 shows these comparisons at high RH region where the confinement impact appears to be more predominant. For each ionomer, compared to the bulk membrane (25-50 μm thick), thin-films on substrates show lower water content ($\lambda_{bulk} > \lambda_{film}$), except PF-AEM and QA-PPO either in I⁻ or Br⁻ counter-anion forms, which possess higher λ in thin-film form

than in bulk membranes ($\lambda_{film} > \lambda_{bulk}$). When comparing the impact of counter-anion on the confinement impact, the correlation falls into the general trend that has been observed for the water content of bulk membranes of $I^- < Br^- < CO_3^{2-}/HCO_3^-$.[31]

For Br^- form QA-PPO, as the side-chain length increases from C0D40 to C16D40 (*i.e.*, $x = 0$ to 16), the higher λ in thin-films than its bulk membrane becomes more significant, especially at low to medium RH (30-70%, Figure 6). In the case of Fumion (Br^-), the membrane water content is much higher than that of thin-film, suggesting that the chemical structure and phase-separation of Fumion (Br^-) may be different from the side-chain functionalized CxxD40 (Br^-). Moreover, the PAP-BP in HCO_3^- form has significant watercontent difference between membrane and thin-film, which could be attributed to the HCO_3^- form membrane possessing relatively higher water content, compared to the membrane having halogen counter ion. [31a]. Meanwhile, the forces resisting swelling of the HCO_3^- form PAP-BP increases as the film thickness decreases due to the stronger confinement effect (the interaction with the substrate and membrane-air interface). As a result, the water content of the bicarbonate form of thin-film becomes significantly smaller than that of the membrane. A similar effect is observed in the highly hygroscopic PFSA membrane (PFSA-H^+) which also showed a high difference in water between the membrane and thin-film.

To further illustrate this effect of confinement, the deviation in water content of thin-films from bulk is described as the ratio: $\frac{\lambda_{Film}}{\lambda_{Bulk}}$. A ratio of less than *1* indicates reduced hydration in an ionomer thin-film compared to its bulk analog ($\lambda_{Film} < \lambda_{Bulk}$). The values for $\frac{\lambda_{Film}}{\lambda_{Bulk}}$ are plotted as a function of the ionomer's IEC and the number of bonds on the side chain (N_B) at various RH conditions to further explore why thin-films exhibit different confinement-driven changes in water content (Table S3 and Figure S6). The values at the high RH (90-99%) and medium RH (50-60%) are shown in Figure 8. Interestingly, the ratio $\frac{\lambda_{Film}}{\lambda_{Bulk}}$ does not correlate well with IEC. In contrast, as shown in Figure 8, the ratio

$\frac{\lambda_{Film}}{\lambda_{Bulk}}$ increases as the ionomer's N_B increases, for both humidity ranges. The dashed lines connecting

two data points for each RH also provide a measure of the range for humidity effect on confinement.

For a given RH, all the $\frac{\lambda_{Film}}{\lambda_{Bulk}}$ values follow a similar trend, demonstrating that as the side-chain size

increases (quantified here by N_B), ionomer uptakes more water in the thin-film form compared to its

bulk analog ($\lambda_{film} > \lambda_{bulk}$). As the N_B decreases, so does the ratio of $\frac{\lambda_{Film}}{\lambda_{Bulk}}$, eventually making some

ionomers absorb less water in thin-film form ($\lambda_{film} < \lambda_{bulk}$). When the same points are plotted against

$N_B \times$ IEC, the observed correlation still holds. Thus, while side-chain chemistry appears to be the

governing factor here, one cannot rule out the secondary effects of IEC. These effects are also illustrated

in Figure 8.

These correlations provide critical information towards understanding of confinement-driven changes in

hydration of ionomer thin-films, which, hitherto, has been established based on Nafion thin-films

exhibiting a reduction in water-uptake in thin-film form.[14b, 15]Thus, one should be careful translating

PEI thin-film phenomenon, especially reduced hydration effects, to other class of ionomers such as

AEIs. Furthermore, these results not only demonstrate that such a confinement effect on AEI/PEI thin-

film hydration is affected by chemistry, but also reveals the possibility of tuning bulk-to-thin-film

variations in AEIs by using side-chain chemistry modifications.

The possible contributions to this phenomenon are:

1) Charge screening impact, the large value of N_B and IEC for PF-AEM and QA-PPO may induce

stronger shielding for the polymer chains from the substrate composition interactions and reduce effects

arising from the substrate or confinement that could cause a deviation in water content from their bulk

analogs.[17a]

2) The local ionic interactions and location of ionic groups, i.e., QA-PPO ionomers have the quaternary ammonium located directly on the backbone and capped with the side chain while other ionomers have a sidechain that is terminated by the functional group.

3) Estimating the functional group frequency in a given volume/environment by multiplying the mass-based IEC with the side-chain "size." Ionomers with a high value of $N_B \times$ IEC exhibit an increase in their hydration upon confinement ($\lambda_{Film} > \lambda_{Bulk}$). PF-AEM with high $N_B \times$ IEC shows comparable uptake as thin-film vs. bulk ($\lambda_{Film} \sim \lambda_{Bulk}$), whereas QA-PPOs with the highest $N_B \times$ IEC show a much higher uptake in thin-film form.

Even though it is difficult to deconvolute these contributions, namely side-chain chemistry vs. ionic identity and IEC, our findings highlight the importance of the combined impact of IEC and side-chain chemistry in controlling the thin-film confinement of ionomers, as illustrated in Figure 8 (bottom), and deviation of hydration from bulk could occur in both directions

3. Discussions

In the following, the collected data are discussed in terms of the effect of ionomer chemistry, backbone hydrocarbon structure, and side-chain chemistry, followed by a summary of different parameters that could guide ionomer design for electrode-ionomer film functionality in fuel cells and electrolyzers for each section.

3.1 Perfluorinated vs. Hydrocarbon

Compared to perfluorinated ionomers, all newly reported hydrocarbon-based ionomers in this study as thin-films lack strong observable phase-separation (no apparent scattering peak, Figure 2), regardless of whether they are cation or anion exchange ionomers as well as their counter-ion type, IEC, and side-chain length. This indicates that the chain flexibility of perfluorinated ionomers promotes the phase-

separation. The impact of phase separation of perfluorinated ionomers on the performance of AEI-based devices has not been thoroughly investigated. However, the thin-film study suggested that the electrodes using the perfluorinated ionomers may have a more heterogeneous structure (locally phase-separated) than the electrode using the hydrocarbon-based ionomers (which are locally mixed with weak phase-separation). In addition, the high mobility of the side chain of the perfluorinated ionomers may form an optimal three-phase interface during the cell break-in process to improve cell performance.[32] On the other hand, the catalyst nanoparticle aggregation in the perfluorinated ionomer bonded electrodes may occur more significantly as the concentration of the ionic groups in the vicinity of the electrocatalysts is higher.[33]

In addition, all the hydrocarbon-based ionomers show a higher solubility parameter (δ), lower density, and relatively low free volume fraction (Figures 4 and 5) than the perfluorinated ionomers (i.e., PFAEM and Nafion). The relatively low free volume fraction observed in hydrocarbon-based ionomers, particularly QA-PPO, can contribute to the lower gas permeability and higher water uptake observed in these ionomers than perfluorinated ones in fuel cells and electrolyzers.[9, 34]

The competing trends between the fraction of free volume and maximum film swelling is depicted in Figure 9. Overall, chemical structures that yield higher swelling in AEI thin-films, which is favorable for ion and water transport, tends to reduce the available free volume, thereby possibly inhibiting gas transport. Despite the limited number of data points, Figure 9 nevertheless provides critical insights for the role of chemistry in electrode-ionomer functionality in alkaline devices. This could be seen clearly in the case of QA-PPO, for which, longer side-chain results in increased swelling at the expense of a slight reduction in free volume. However, N2-25 and QS exhibit comparable swelling to QA-PPO but possess higher free volume indicating better gas transport functionality at the given IEC.

3.2 Aliphatic vs. Aromatic Backbone

Next, we examine hydration and solubility differences of amorphous hydrocarbon ionomers with aliphatic and aromatic backbones (Figure 4). Compared to aromatic backbones (i.e., DMBPN, PAP-BP, QA-PPO, and Fumion), aliphatic backbone ionomers (i.e., N2-25, QS, and PSS) show relatively high solubility parameter (δ) likely due to their stronger molecular cohesive forces.[22] The δ of aliphatic backbone ionomers is closer to that of water (48 MPa$^{1/2}$), generally resulting in a higher degree of water uptake; however, a stiffer structure can result in lower swelling for a similar solubility parameter (e.g., QA-PPO and QS). In addition, aliphatic backbone polystyrene chemistry-based N2-25 and QS enable them to possess a higher free volume fraction and water content (Figure 5). While the relationship between the hydration and solubility parameter may exist in both bulk and thin-film geometries, we have further shown the thin-film confinement effect on hydration, which is more relevant to the gas and ion transport.[35]

Considering that hydration is the key factor governing ion transport in amorphous AEMs,[35] effect of chemistry on hydration effect could be extended to ion transport functionalities as well. On one hand, higher water uptake AEIs could possibly lead to anode flooding and higher sensitivity to humidification. This can explain the higher performance in AEMFCs when the ionomers are mixed in the form of particles.[36] On the other hand, higher water uptake of aliphatic AEIs may be advantageous for AEMWE applications, in which reactant water can be supplied without mass transport limitation under high hydrogen-generating conditions. Aromatic backbone-based DMBPN possesses high IEC yet relatively low water uptake, which may explain reduced flooding observed in the electrode alongside the low water transport in fuel cells.[37]

3.3 Side-chain Conformation

The side-chain composition is an important parameter in controlling the transport properties, water uptake, chemical stability, and morphology of bulk ionomer membranes.[14a, 38] For example, shorter side-chain length PFSA showed more tortuous ion transport pathways than Nafion.[38a, 38b] A long side-chain carbon spacer was found to enhance the alkaline chemical stability of AEM.[38c] Significant higher degree of crystallinity was found in the shorter side-chain length of graft copolymer membranes.[39] For the ionomer thin-films in this study, side-chain chemistry influences their properties as listed below:

(i) The nanostructure of perfluorinated ionomers (Figure 2, PF-AEM vs. Nafion): for comparable IECs, PF-AEM exhibits larger d-spacing (~5-6 nm) in both parallel and perpendicular to substrate directions at high RH, due to the formation of larger ionic aggregation, which could be attributed to longer side-chain and its high flexibility in the PF-AEM.[20a] In addition, the d-spacing of Nafion and PF-AEM both increases with hydration, which alludes to nano-swelling phenomena occurring in perfluorinated ionomers as compared to hydrocarbon ones. Compared to Nafion, PF-AEM films also possesses higher swelling and water content.

(ii) Ionomer density decreases with increasing side-chain length (Figure 5 and 9), e.g., QA-PPO (from C0D40 to C16D40) as well as Nafion vs. PF-AEM, which could be due to their longer side-chains hindering the close packing of the polymer chains. These results unravel insights for prediction molecular packing of ionomers. Similarly, the free volume fraction of ionomers increases with side-chain length, which could provide critical information for determining their gas transport[40] and thermal transition temperature.[41]

(iii) The confinement impact for thin-films. PFAEM shows higher water content in thin-film form than their bulk free-standing membranes. This effect of confinement is similar to the results previously reported for QA-PPO.[17a] The combined impact of IEC and side-chain length (Figure 8) could be responsible for the confinement impact in these ionomers, where these AEMs become less attracted to the substrate in comparison to highly attractive

interactions observed in PFSAs. These findings suggest that the PF-AEM could be suitable as the cathode ionomer for which a high hydration level is required.

3.4 Functional Groups and Counter-anions

Converting all the AEI thin-films into the same counter anions was observed to be very challenging due to the delamination of supported thin-films during anion-exchange or casting process. For this reason, our AEI thin-films were kept primary in Br^- and HCO_3^- forms. Compared to I^- form (PF-AEM), these counter-ions show strong hydration-confinement interplay. The trend follows roughly $I^- < Br^- < HCO_3^-$,which was previous observed in the hydration of bulk AEMs and attributed to the difference in the ion dissolution enthalpies.[31b]

Regarding cation structure, there are several notable impacts on water uptake of the thin film. First, hydrophobic ethyl ammonium functionalized polymer (QS) has relatively low water uptake than methylammonium functionalized polymers (N2-25) in spite of the high IEC of the former. This additional effect may cause some deviations in the solubility parameter vs. swelling shown in Figure 4. Second, polymer backbone tethered piperidinium polymer (PAP-BP) has suppressed water uptake at high RH in spite of the high IEC (2.88 meq g^{-1}). In other words, the hydration at low RH is relatively high, a possible benefit of high hydroxide conductivity at low RHs. This unique water swelling behavior of PAP-BP is probably due to the hydrophobic bulky piperidinium cations are directly tethered to the rigid backbone. It may provide improved conductivity and stability at higher temperature operation, which is consistent with the previous reports on their performance.[9] Third, adding multiple cations per side-chain site (N2-25) has very high water uptake at high RH (Figure 4). Adding multiple cations per side-chain site has been adopted as a design strategy to boost the ion conductivity and tune the nano-phase separation of ionomers.[42], [7b, 43] N2-25 with dual-cation on the side-chain exhibits a higher solubility parameter, larger swelling, and greater water content than single cation polymers in spite of the relatively lower IEC. Thus, multi-cation groups on the side chain could be an effective strategy for

enhancing the hydroxide conduction of AEI thin-films under hydrated conditions. This result is consistent with result that showed significantly larger ion conductivity for multi-cation ionomers compared to the polymers with one functional group per side-chain site.[7b, 42a, 43b, 44] Our finding of enhanced hydration of multi-functionalized ionomer could be a reason for their improved ion conductivity. On the other hand, AEIs with low hydration (DMBPN, QS, Fumion, and C16D40) could be viable candidates for electrodes that require ionomers with lower hydration and stronger catalyst binding, such as AEMFC anode.[37]

4. Conclusions and Outlook

We have investigated hydration, nano-structure, ionomer density, and confinement impact of anion exchange ionomer thin-films with various backbones and side-chain chemistries and compared with proton exchange ionomer thin-films.

The ionomer chemistry is found to have a strong impact on ionomers' properties. In terms of chemistry effect on morphology, thin-films with perfluorinated backbone exhibit nano-phase separation, regardless of whether they have fixed anion or cations groups. In contrast, all hydrocarbon-based ionomer thin-films studied herein have no detectable degree of nano-phase separation. PFAEM with the longer side-chain also results in better phase-separation. Thus, the dissimilarity of the backbone and side-chain is one of the key factors promoting the nano-phase-separation of ionomer domains.

In terms of the effect of chemistry on hydration and other properties, compared to perfluorinated ionomers, hydrocarbon-based ionomers exhibit higher solubility parameters, smaller density, and lower calculated free volume fraction. For hydrocarbon AEIs, the aliphatic backbone increases the solubility parameter further compared to aromatic backbones. As the side-chain length increases, ionomer density decreases. Moreover, N2-25 has a higher solubility parameter and greater water content than QS, owing to its multifunctional base groups on its side-chain. The ionomer solubility parameter is found to be

critical to the ionomer swelling. The combined effect of IEC and bond number on side-chain, as well as the counter-ions are important factors rendering the degree of confinement in ionomers.

Given the crucial role of water in electrode performance of AEM based devices, our exploration of confinement phenomena and hydration for AEI thin-films would give significant insight into designing AEI ionomers for electrodes and device water management. Particularly, our findings that the water uptake of some AEIs in thin-film form can actually be higher than that in the bulk polymer (membrane) is a significant expansion of the current understanding of ionomer function in electrode, which rely primarily on PFSA PEIs. So, AEIs with long side-chain tethered poly(phenylene oxide) can hydrate more in thin-film form, in sharp contrasts to PFSA PEI systems. Moreover, confinement-driven changes in hydration can be modulated using chemistry and IEC, with the size of the side-chain being the key parameter. These observations may provide an explanation for the electrode flooding and relatively low cell ohmic resistance of AEMFCs using long alkyl chain tethered AEI. More importantly, the findings herein underscore the role of chemistry in tuning the functionality of ionomer thin-films and the confinement-anion interplay and, therefore, provide guidance for the design of next-generation ionomers for the electrodes of alkaline fuel cells, electrolyzers, and other electrochemical systems, wherein thin-films provide critical transport functionalities.[37]

5. Experimental
5.1 Materials
Ten AEIs and two PEIs used in this study are shown in Table 1. PF-AEM (received from National Renewable Energy Laboratory, Golden, Co), PAP-BP-60 (received from University of Delaware, Newark, DE), and other three ionomers (N2-25, QS, and DMBPN received from Los Alamos National Laboratory, Los Alamos, NM) were abbreviated as PF-AEM, PAP, N2-25, QS, and DMBPN, respectively. Previously reported materials QA-PPO[17a] were also used in this study. The QA-PPO

(CxD40) with various side-chain lengths (x=1, 6, 10, 16) are abbreviated as C0D40, C6D40, C10D40, C16D40, respectively. Commercially available Fumion® (Fumatech, Fuel Cell Store) was used as a baseline for AEIs. Two proton exchange ionomer (PEI) dispersions were also used for comparison. Poly(4-styrenesulfonic acid) (PSS) and Nafion D521 were purchased from Sigma-Aldrich and Fuel Cell Store, respectively.

5.2 Thin-film Preparation

Various AEI dispersions were prepared as stock solutions for casting. The stock AEI dispersion was diluted to desired concentrations by adding solvents (Sigma Aldrich), as shown in Table S1. The diluted solutions were stirred overnight, sonicated for 60 min, and filtered using PTFE syringes and filters (0.45 μm pore size, VWR) to avoid dissolving by organic solvent during the filtration procedure before spin-casting. AEI concentrations were prepared based on the thin-film thickness and dispersion concentration correlations for each polymer dispersion system, as shown in Figure S 1. Concentrations were determined to achieve a target dry thickness of 35 ± 5 nm.

AEI thin-film casting requires a very clean and scratch-free substrate. Cleaning and handling the substrate was challenging and needed extra care compared to the regular PEI thin-film[15a] substrate procedure (see SI for details). Prior to spin casting, the silicon wafer substrates were washed with alcohol solvents to remove the surface contamination and then submerged in 200 proof ethanol solution and placed in a sonication bath for 30 min to further clean the substrates. The substrates were then carefully removed from the solvent bath and rinsed with isopropyl alcohol, followed by rinsing with DI water (Millipore, 18 MΩ-cm). The polished silicon wafers were placed vertically to prevent any scratches from obtaining high-quality surfaces on both sides of the substrate. Substrates were dried under a dry nitrogen stream and placed in a plasma cleaner (PDC-001, Harrick Plasma) chamber for 30 min.

Spin-cast films were prepared by dropping 50 μL of the solution on a substrate at rest after N_2 purged the casting chamber for 1 min to dry the air, and then the sample was immediately spun at 4000 rpm for

one minute. After the rotation returned to rest, the samples were then placed under flowing dry air for further drying, followed by drying at 70 °C under vacuum overnight. Obtaining similar counter-ions for all AEI thin-films by anion-exchange caused significant problems with casting and delamination, restricting this investigation to certain anion forms (see SI for the details).

5.3 Grazing-Incidence Small-Angle X-Ray Scattering (GISAXS)

GISAXS measurements were performed as described previously in the literature.[14b, 15a] Thin-film samples were placed into an in-house built environmental chamber with X-ray transparent Kapton windows. The samples were equilibrated at 95% RH at room temperature (25°C) for at least 30 minutes. All the GISAXS patterns presented here were collected at an incidence angle (α) above the critical angle for ionomer thin-films, but below that for the substrate (i.e., $\alpha = 0.2$ for SiO_2) and varied within the range of 0.16 to 0.20. All GISAXS experiments were performed at beamline 7.3.3 of the Advanced Light Source (ALS) at Lawrence Berkeley National Laboratory (LBNL). The sample to detector distance was approximately 1.8 m for the GISAXS configuration. Exposure time for the collected images was 10 s. The X-ray energy used was 10 keV, with a monochromator energy resolution E /d E of 100, and the patterns are shown were acquired with a 2D Dectris Pilatus 2M CCD detector (172 μm $\times$ 172 μm pixel size). The 1-D intensity profiles were extracted from the 2D images using vertical and horizontal line cuts.

5.4 Thickness Swelling

The hydration behavior of thin films was characterized by spectroscopic ellipsometry, as described previously for PEI thin films.[14b, 15a] Film thicknesses were measured in-situ by varying relative humidity (RH) using a J.A. Woollam alpha-SE spectroscopic ellipsometer (Lincoln, NE) and N_2 as humidifying gas at a flow rate of 500 sccm for all set points. Samples were initially exposed to 30 min of 0% and 100% RH, respectively, for preconditioning. The changes in the wave amplitude (Ψ) and phase shift (Δ) were measured over a spectral range of 300 to 900 nm (1.4–4.15 eV) and then

characterized using a Cauchy layer to derive the thickness and optical properties of the polymer films on optically characterized substrates. The change in thickness and complex refractive index was calculated for films exposed to varying RH increments from 0 to 100 % RH in an in-house constructed environmental cell held at ambient temperature. The cell was made with non-polarizing fused silica windows to maximize the amount of light transmitted. Thin-film thickness at a given RH, L_{RH}, is the average thickness after the sample reaches equilibrium. The dry thickness (L_0) was measured after the film is equilibrated at 0% RH. The change in thickness (ΔL) was used to calculate through-plane swelling as follows:

$$\text{Swelling Fraction (\%)} = \frac{\Delta L}{L_0} \times 100\% \tag{4}$$

5.5 Water-Uptake and Polymer Film Density

QCM measurements were carried out with a Maxtex RQCM monitor. The QCM crystal baseline frequency was recorded prior to spin coating. Blank QCM/ellipsometry measurements at 0% and 95% RH were taken to determine the porosity of each substrate and corrected for water adsorption in SiO_2 nanopores.[45] An RH profile from 0-95% RH was conducted on one of the blank SiO_2 crystals in 10% RH increments of 15 minutes at low RH and 30 minutes at elevated RH to allow for interpolation of full RH profiles for each of the QCM substrates. Water uptake was calculated from QCM data using the Sauerbrey equation (Equation 5) assuming linear elastic behavior in the thin-film regime:

$$\Delta f = -\frac{2f_0^2}{A\sqrt{\rho_q \mu_q}} \Delta m \tag{5}$$

where Δf is the change in frequency, f_0 is the fundamental frequency of the uncoated crystal, A (= 0.402 cm²) is the active area, and ρ_q (= 2.648 g cm⁻³) and μ_q (= 2.947 × 10¹¹ g cm⁻¹ s⁻²) are the density and shear modulus of the QCM crystal, respectively. The water uptake measured from QCM was calculated by subtracting the mass of water absorbed into the SiO_2 nanopores from the total mass, to obtain:

$$\text{Water Uptake (\%)} = \frac{\Delta m - m_{SiO2}}{m_0 - m_{SiO2}} \times 100\% \tag{6}$$

where Δm, m_0 and m_{SiO2} are the mass change, initial dry mass of the film, and mass of water in the

SiO$_2$, respectively. Local water content, λ was calculated using Equation 7:

$$\lambda = \frac{\Delta m}{M_{H_2O} \times IEC} \tag{7}$$

where M_{H_2O} is the molar mass of water; IEC is the ion exchange capacity of ionomer dispersion.

The density of the dry ionomer (ρ_p) on the substrate was obtained from the slope of the line created

when the swelling plotted against water uptake, as shown in S2. Assuming one-dimensional swelling,

the correlation of swelling fraction and water uptake is shown below:

$$\frac{\Delta m}{m_p} = \frac{\rho_w \Delta V_w}{\rho_p V_p} \equiv \frac{\rho_w \Delta L}{\rho_p L_0} = \frac{1}{\rho_p} \frac{\Delta L}{L_0} \tag{8}$$

where m_p, ρ_p and V_p are the dry mass, dry density, and dry volume of the film, respectively. Δm, ρ_w,

and ΔV_w are the mass, density (1 g cm^{-3}), and volume of water absorbed in the film, respectively.

Supporting Information
Supporting Information is available from the Wiley Online Library or from the author.

Conflict of Intrest
The authors declare no conflict of interest.

Acknowledgements

References

[1]   J. R. Varcoe, P. Atanassov, D. R. Dekel, A. M. Herring, M. A. Hickner, P. A. Kohl, A. R. Kucernak, W. E. Mustain, K. Nijmeijer, K. Scott, T. Xu, L. Zhuang, *Energy & Environmental Science* **2014**, 7, 3135.

[2]   a) D. R. Dekel, *Journal of Power Sources* **2018**, 375, 158; b) S. Gottesfeld, D. R. Dekel, M. Page, C. Bae, Y. Yan, P. Zelenay, Y. S. Kim, *Journal of Power Sources* **2018**, 375, 170.

[3]   H. A. Miller, K. Bouzek, J. Hnat, S. Loos, C. I. Bernäcker, T. Weißgärber, L. Röntzsch, J. Meier-Haack, *Sustainable Energy & Fuels* **2020**, 4, 2114.

[4]   D. P. Leonard, S. Maurya, E. J. Park, L. Delfin Manriquez, S. Noh, X. Wang, C. Bae, E. D. Baca, C. Fujimoto, Y. S. Kim, *Journal of Materials Chemistry A* **2020**, 8, 14135.

[5]   D. Li, E. J. Park, W. Zhu, Q. Shi, Y. Zhou, H. Tian, Y. Lin, A. Serov, B. Zulevi, E. D. Baca, C. Fujimoto, H. T. Chung, Y. S. Kim, *Nature Energy* **2020**, 5, 378.

[6]   a) J. Pan, C. Chen, Y. Li, L. Wang, L. Tan, G. Li, X. Tang, L. Xiao, J. Lu, L. Zhuang, *Energy & Environmental Science* **2014**, 7, 354; b) J. Ran, L. Wu, B. Wei, Y. Chen, T. Xu, *Scientific Reports* **2014**, 4, 6486; c) E. A. Weiber, P. Jannasch, *ChemSusChem* **2014**, 7, 2621; d) E. A. Weiber, D. Meis, P. Jannasch, *Polym Chem-Uk* **2015**, 6, 1986; e) N. Li, L. Wang, M. Hickner, *Chemical Communications* **2014**, 50, 4092; f) J. Si, S. Lu, X. Xu, S. Peng, R. Xiu, Y. Xiang, *Chemsuschem* **2014**, 7, 3389.

[7]   a) J. Fan, A. G. Wright, B. Britton, T. Weissbach, T. J. G. Skalski, J. Ward, T. J. Peckham, S. Holdcroft, *ACS Macro Lett.* **2017**, 6, 1089; b) L. Zhu, J. Pan, Y. Wang, J. Han, L. Zhuang, M. A. Hickner, *Macromolecules* **2016**, 49, 815.

[8]   W. E. Mustain, M. Chatenet, M. Page, Y. S. Kim, *Energy & Environmental Science* **2020**, DOI: 10.1039/D0EE01133A.

[9]   J. Wang, Y. Zhao, B. P. Setzler, S. Rojas-Carbonell, C. Ben Yehuda, A. Amel, M. Page, L. Wang, K. Hu, L. Shi, S. Gottesfeld, B. Xu, Y. Yan, *Nature Energy* **2019**, DOI: 10.1038/s41560-019-0372-8.

[10]   a) L. Wang, M. Bellini, H. A. Miller, J. R. Varcoe, *Journal of Materials Chemistry A* **2018**, 6, 15404; b) T. J. Omasta, A. M. Park, J. M. LaManna, Y. Zhang, X. Peng, L. Wang, D. L. Jacobson, J. R. Varcoe, D. S. Hussey, B. S. Pivovar, W. E. Mustain, *Energ Environ Sci* **2018**, 11, 551.

[11]   S. Maurya, S. Noh, I. Matanovic, E. J. Park, C. Narvaez Villarrubia, U. Martinez, J. Han, C. Bae, Y. S. Kim, *Energy & Environmental Science* **2018**, 11, 3283.

[12]   a) F. Barbir, *Solar Energy* **2005**, 78, 661; b) M. S. Cha, J. E. Park, S. Kim, S.-H. Han, S.-H. Shin, S. H. Yang, T.-H. Kim, D. M. Yu, S. So, Y. T. Hong, S. J. Yoon, S.-G. Oh, S. Y. Kang, O.-H. Kim, H. S. Park, B. Bae, Y.-E. Sung, Y.-H. Cho, J. Y. Lee, *Energy & Environmental Science* **2020**, DOI: 10.1039/D0EE01842B.

[13]   A. M. Park, Z. R. Owczarczyk, L. E. Garner, A. C. Yang-Neyerlin, H. Long, C. M. Antunes, M. R. Sturgeon, M. J. Lindell, S. J. Hamrock, M. Yandrasits, B. S. Pivovar, *ECS Transactions* **2017**, 80, 957.

[14]   a) A. Kusoglu, A. Z. Weber, *Chemical Reviews* **2017**, 117, 987; b) A. Kusoglu, D. Kushner, D. K. Paul, K. Karan, M. A. Hickner, A. Z. Weber, *Advanced Functional Materials* **2014**, 24, 4763.

[15]   a) A. Kusoglu, T. J. Dursch, A. Z. Weber, *Advanced Functional Materials* **2016**, 26, 4961; b) K. Karan, *Langmuir : the ACS journal of surfaces and colloids* **2019**, 35, 13489.

[16]   X. Luo, A. Wright, T. Weissbach, S. Holdcroft, *Journal of Power Sources* **2018**, 375, 442.

[17]   a) D. I. Kushner, L. Zhu, A. Kusoglu, M. A. Hickner, *Macromolecular Chemistry and Physics* **2016**, 217, 2442; b) V. J. Bharath, J. Millichamp, T. P. Neville, T. J. Mason, P. R. Shearing, R. J. C. Brown, G. Manos, D. J. L. Brett, *J. Membr. Sci.* **2016**, 497, 229; c) V. J. Bharath, J. R. Jervis, J. J. Bailey, E. Engebretsen, T. P. Neville, J. Millichamp, T. Mason, P. R. Shearing, R. J. C. Brown, G. Manos, D. J. L. Brett, *International Journal of Hydrogen Energy* **2017**, 42, 24301.

[18]   D. I. Kushner, A. Kusoglu, N. J. Podraza, M. A. Hickner, *Advanced Functional Materials* **2019**, 29, 1902699.

[19]   a) F. S. Bates, G. H. Fredrickson, *Annual Review of Physical Chemistry* **1990**, 41, 525; b) F. S. Bates, G. H. Fredrickson, *Physics Today* **1999**, 52, 32.

[20] a) A. Eisenberg, B. Hird, R. B. Moore, *Macromolecules* **1990**, 23, 4098; b) A. Eisenberg, *Macromolecules* **1970**, 3, 147.

[21] a) J. Y. Park, D. R. Paul, *Journal of Membrane Science* **1997**, 125, 23; b) J. Marrero, R. Gani, *Fluid Phase Equilibria* **2001**, 183-184, 183; c) X. Yan, Q. Dong, X. Hong, *Journal of Chemical & Engineering Data* **2003**, 48, 374.

[22] R. F. Fedors, *Polymer Engineering & Science* **1974**, 14, 147.

[23] W. H. Ferrell, D. I. Kushner, M. A. Hickner, *Journal of Polymer Science Part B: Polymer Physics* **2017**, 55, 1365.

[24] U. N. Shrivastava, H. Fritzsche, K. Karan, *Macromolecules* **2018**, 51, 9839.

[25] A. Kusoglu, K. Vezzù, G. A. Hegde, G. Nawn, A. R. Motz, H. N. Sarode, G. M. Haugen, Y. Yang, S. Seifert, M. A. Yandrasits, S. Hamrock, C. M. Maupin, A. Z. Weber, V. Di Noto, A. M. Herring, *Chemistry of Materials* **2020**, 32, 38.

[26] a) Y. Yu, Y. Wang, T. Li, W. Liang, C. Li, W. Niu, L. Gao, *RSC Advances* **2017**, 7, 42468; b) Y. P. Yampolskii, A. P. Korikov, V. P. Shantarovich, K. Nagai, B. D. Freeman, T. Masuda, M. Teraguchi, G. Kwak, *Macromolecules* **2001**, 34, 1788.

[27] A. Katzenberg, A. Chowdhury, M. Fang, A. Z. Weber, Y. Okamoto, A. Kusoglu, M. A. Modestino, *Journal of the American Chemical Society* **2020**, 142, 3742.

[28] L. A. Zook, J. Leddy, *Analytical Chemistry* **1996**, 68, 3793.

[29] D. W. Van Krevelen, in *Properties of Polymers (Third Edition)*, DOI: https://doi.org/10.1016/B978-0-444-82877-4.50011-1 (Ed: D. W. Van Krevelen), Elsevier, Amsterdam **1997**, p. 71.

[30] A. Bondi, *The Journal of Physical Chemistry* **1964**, 68, 441.

[31] a) W. Germer, J. Leppin, C. Nunes Kirchner, H. Cho, H.-J. Kim, D. Henkensmeier, K.-Y. Lee, M. Brela, A. Michalak, A. Dyck, *Macromolecular Materials and Engineering* **2015**, 300, 497; b) M. G. Marino, J. P. Melchior, A. Wohlfarth, K. D. Kreuer, *J. Membr. Sci.* **2014**, 464, 61.

[32] X. Lin, C. M. Zalitis, J. Sharman, A. R. J. Kucernak, *ACS Applied Materials & Interfaces* **2020**, DOI: 10.1021/acsami.0c12718.

[33] Y. S. Kim, C. F. Welch, N. H. Mack, R. P. Hjelm, E. B. Orler, M. E. Hawley, K. S. Lee, S. D. Yim, C. M. Johnston, *Physical Chemistry Chemical Physics* **2014**, 16, 5927.

[34] C. Klose, T. Saatkamp, A. Münchinger, L. Bohn, G. Titvinidze, M. Breitwieser, K.-D. Kreuer, S. Vierrath, *Advanced Energy Materials* **2020**, 10, 1903995.

[35] a) X. Luo, S. Rojas-Carbonell, Y. Yan, A. Kusoglu, *Journal of Membrane Science* **2019**, 598, 117680; b) J. Lu, A. Barnett, V. Molinero, *The Journal of Physical Chemistry C* **2019**, 123, 8717; c) G. A. Giffin, S. Lavina, G. Pace, V. Di Noto, *The Journal of Physical Chemistry C* **2012**, 116, 23965.

[36] B. S. Pivovar, *DOE Hydrogen and Fuel Cells Program Annual Merit Review and Peer Evaluation Meeting* **2018**.

[37] E. J. Park, S. Maurya, A. S. Lee, D. P. Leonard, D. Li, J. Y. Jeon, C. Bae, Y. S. Kim, *Journal of Materials Chemistry A* **2019**, 7, 25040.

[38] a) K. D. Kreuer, M. Schuster, B. Obliers, O. Diat, U. Traub, A. Fuchs, U. Klock, S. J. Paddison, J. Maier, *J. Power Sources* **2008**, 178, 499; b) X. Luo, S. Holdcroft, A. Mani, Y. Zhang, Z. Shi, *Physical Chemistry Chemical Physics* **2011**, 13, 18055; c) K. M. Meek, J. R. Nykaza, Y. A. Elabd, *Macromolecules* **2016**, 49, 3382.

[39] A. C. C. Yang, R. Narimani, Z. Zhang, B. J. Frisken, S. Holdcroft, *Chemistry of Materials* **2013**, 25, 1935.

[40] a) C. Nagel, K. Günther-Schade, D. Fritsch, T. Strunskus, F. Faupel, *Macromolecules* **2002**, 35, 2071; b) D. Saha, H. A. Grappe, A. Chakraborty, G. Orkoulas, *Chemical Reviews* **2016**, 116, 11436.

[41] a) R. P. White, J. E. G. Lipson, *Macromolecules* **2016**, 49, 3987; b) Y. U. S. Lipatov, V. P. Privalko, *Journal of Macromolecular Science, Part B* **1973**, 7, 431.

[42] a) D. Guo, C. X. Lin, E. N. Hu, L. Shi, F. Soyekwo, Q. G. Zhang, A. M. Zhu, Q. L. Liu, *Journal of Membrane Science* **2017**, 541, 214; b) A. Kusoglu, K. Vezzu, G. A. Hegde, G. Nawn, A. R.

Motz, H. N. Sarode, G. M. Haugen, Y. Yang, S. Seifert, M. A. Yandrasits, S. Hamrock, C. M. Maupin, A. Z. Weber, V. Di Noto, A. M. Herring, *Chemistry of Materials* **2020**, 32, 38; c) G. M. Su, I. A. Cordova, M. A. Yandrasits, M. Lindell, J. Feng, C. Wang, A. Kusoglu, *J Am Chem Soc* **2019**, 141, 13547.

[43]   a) Y. He, J. Si, L. Wu, S. Chen, Y. Zhu, J. Pan, X. Ge, Z. Yang, T. Xu, *Journal of Membrane Science* **2016**, 515, 189; b) J. Wang, S. Gu, R. Xiong, B. Zhang, B. Xu, Y. Yan, *ChemSusChem* **2015**, 8, 4229.

[44]   a) X. L. Gao, Q. Yang, H. Y. Wu, Q. H. Sun, Z. Y. Zhu, Q. G. Zhang, A. M. Zhu, Q. L. Liu, *Journal of Membrane Science* **2019**, 589, 117247; b) Y. He, L. Wu, J. Pan, Y. Zhu, X. Ge, Z. Yang, J. Ran, T. Xu, *Journal of Membrane Science* **2016**, 504, 47.

[45]   D. I. Kushner, M. A. Hickner, *Langmuir* **2017**, 33, 5261.
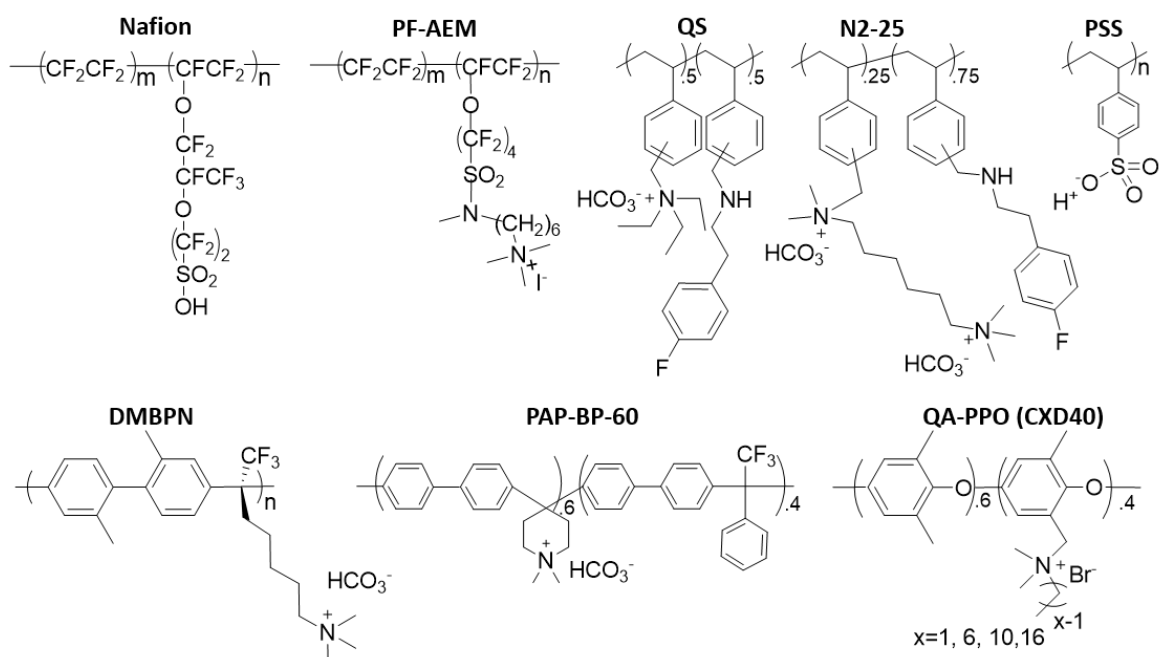
**Figure 1.** The chemical structure of ionomers investigated in this study.
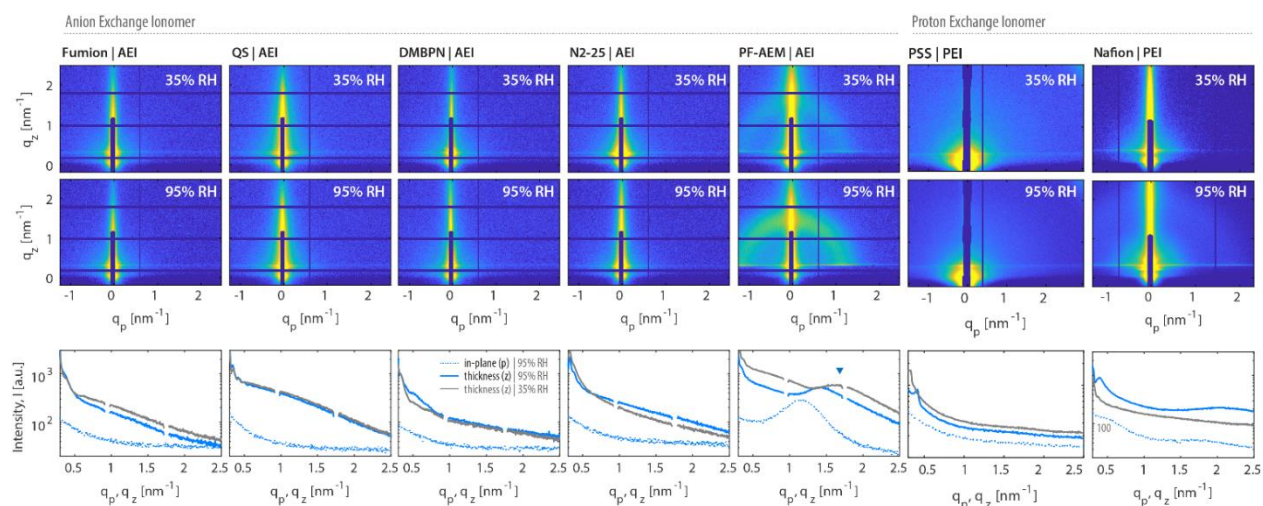
Figure 2. 2D GISAXS patterns for Fumion, QS, DMBPN, N2-25, PF-AEM and PAP-BP, Nafion and PSS ionomer thin-films with a thickness of 30-40 nm (measured at 0% RH) on silicon substrates in ambient and vapor-saturated environment. Corresponding line cuts in q_p and q_z directions are shown below.
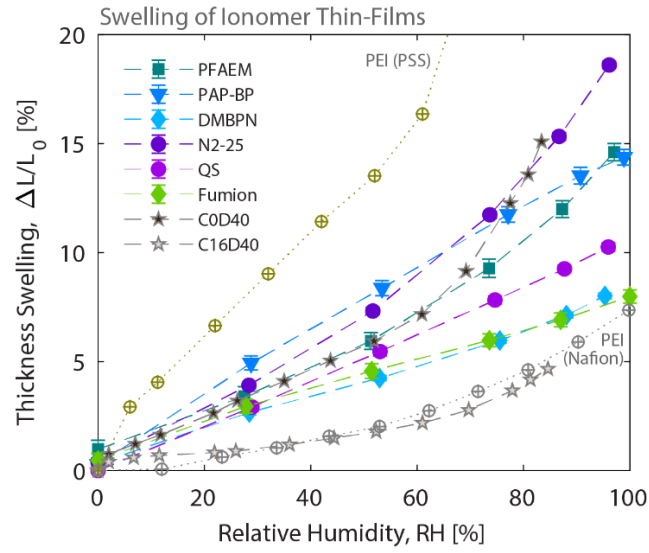
Figure 3. Thickness swelling of AEI and PEI thin-films (30-100 nm thick) as a function of RH, measured by environmental ellipsometry. Data for QA-PPO (CXD40 series) is retrieved from ref.[17a].
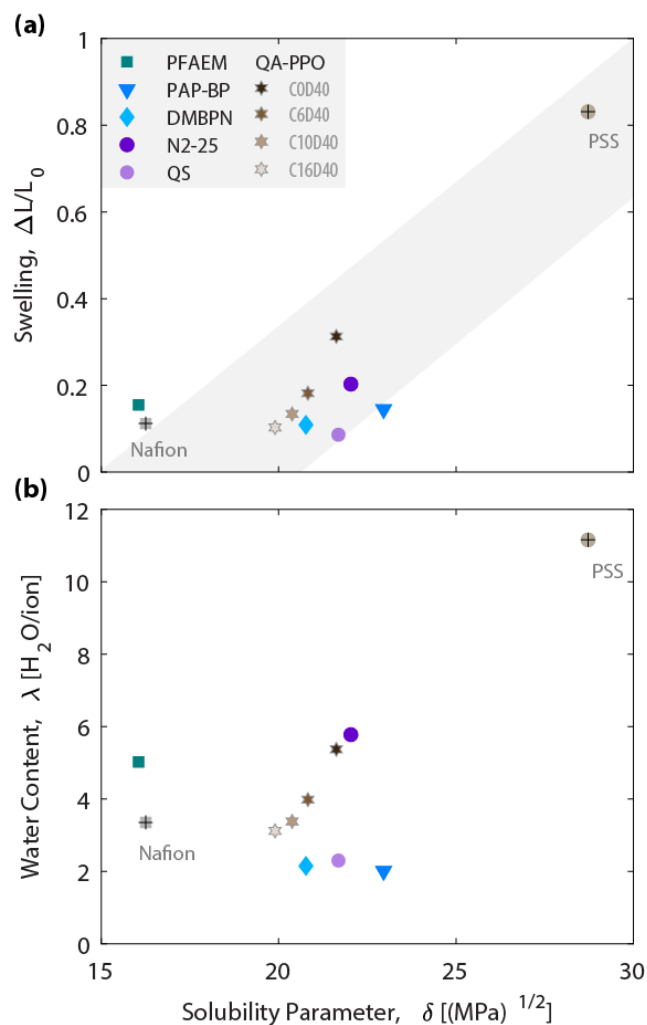
Figure 4. (a) Thickness swelling and (b) water content per ionic group of thin films measured at 100% RH plotted as a function of calculated solubility parameter using group contribution method (see SI for details). Thickness values of the films (in 30-100 nm range) are listed in Figure S1.
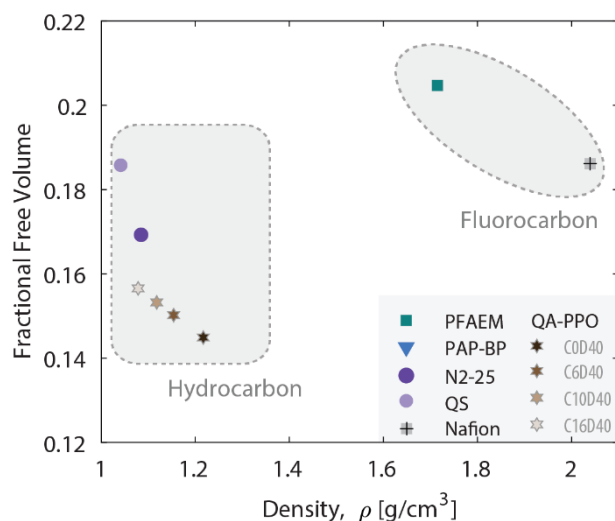
Figure 5. The calculated free volume fraction as a function of density for hydrocarbon and perfluorinated ionomers. Thickness of the films are the same as in Figure 4.
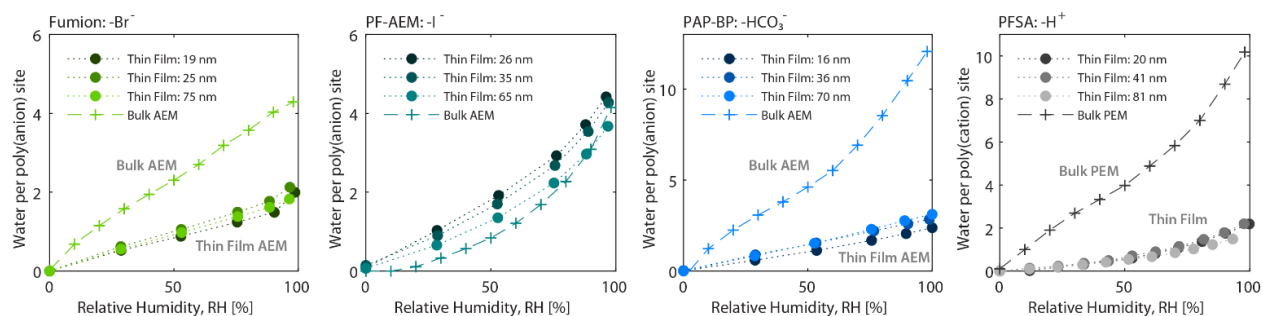

Figure 6. Comparison of humidity-dependent water uptake behavior of ion-exchange ionomer in thin-films (spin-cast on Si) vs. its bulk membrane analogue for (a) Fumion AEM (Br form), (b) PF-AEM (I form), (c) PAP-BP (bicarbonate form), and (d) PFSA PEM.
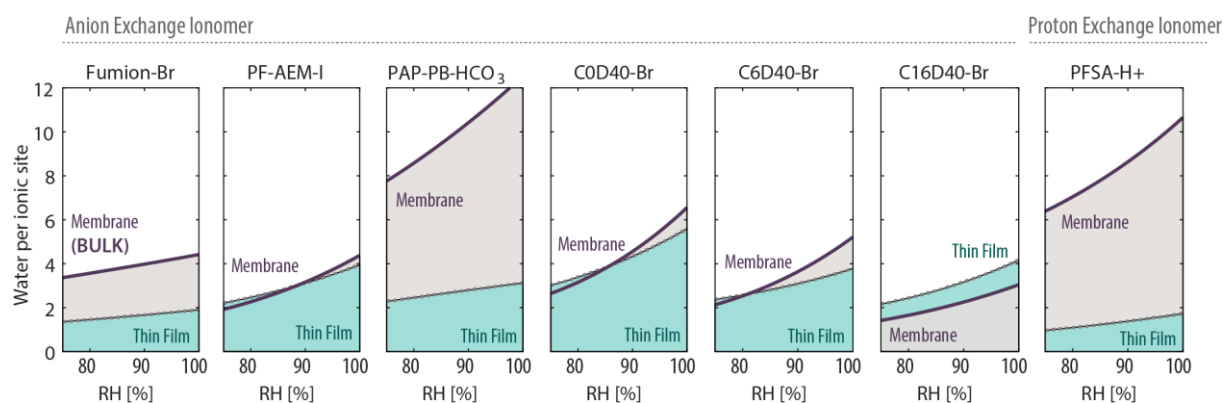
Figure 7. The confinement impact on ionomers: Comparison of the water content of ion-exchange ionomer in thin-films (spin-cast on Si) vs. its bulk membrane analogue in high-humidity region. (The trends are generated by fitting to experimental data in Figure 6 using bulk membranes and thin-films in the thickness range of 65-81 nm).
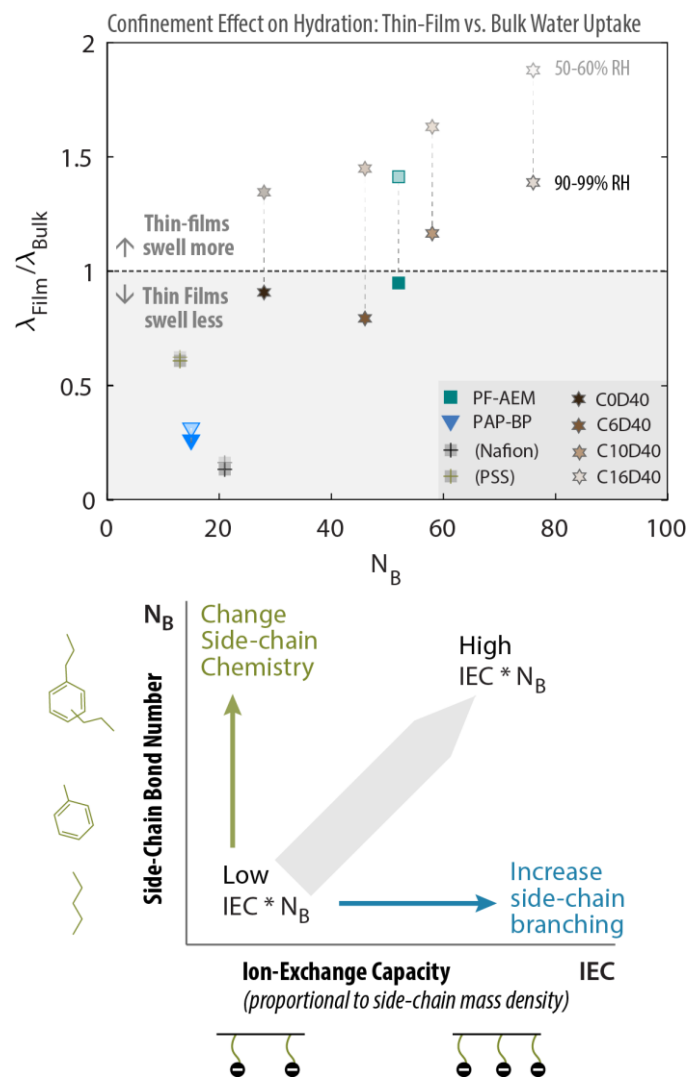
Figure 8. Confinement-driven deviations in maximum water content of ionomer thin films from bulk behavior in terms of $\lambda_{Film}/\lambda_{Bulk}$ plotted against the bond number of side-chain (N_B). Open and closed symbols represent conditions of medium RH 50-60% and high (90-99%), respectively. (bottom) The schematic below illustrates the role of each parameter and their combined effect on the confinement effect.
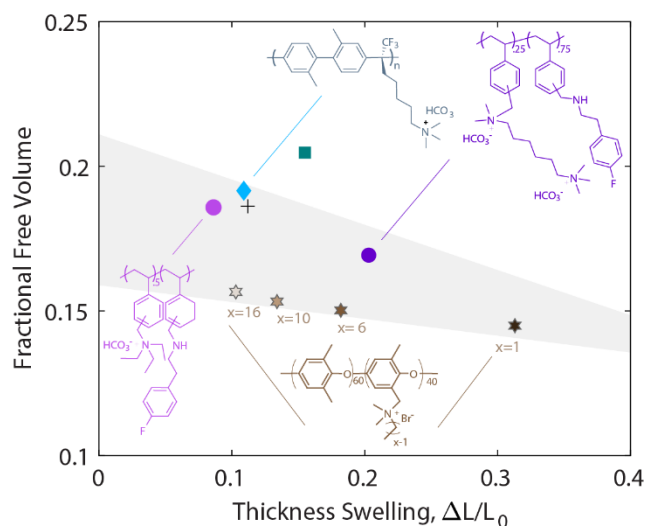
Figure 9. Multi-functionality of AEIs bounded by the free volume fraction of thin-films determined in dry state vs. their maximum thickness swelling at $95 \pm 2\%$ RH. (+) represents PEI Nafion thin-film (proton form) and included to provide a comparison.

Table 1. Characteristics of ionomers used in this work.

Ionomer Sample	Ion exchange capacity (meq g^{-1})	Counter-ion
AEI		
PF-AEM	1.0	I$^-$
PAP-BP-60	2.9	HCO$_3^-$
QS	2.0	HCO$_3^-$/CO$_3^{2-}$
N2-25	1.8	HCO$_3^-$/CO$_3^{2-}$
DMBPN	2.5	HCO$_3^-$/CO$_3^{2-}$
C0D40	2.7	Br$^-$
C6D40	2.2	Br$^-$
C10D40	2.0	Br$^-$
C16D40	1.7	Br$^-$
Fumion®	1.7	Br$^-$
PEI		
Nafion	0.9	H$^+$
PSS	2.8	H$^+$